International Journal of Refractory Metals and Hard Materials 95 (2021) 105447

Contents lists available at ScienceDirect

International Journal of Refractory Metals and Hard Materials

journal homepage: www.elsevier.com/locate/IJRMHM

Microstructure and mechanical properties of liquid–phase sintered W@NiFe composite powders

Nan Deng [a,b], Jianqiang Li [b], You Wang [a], DanDan Qu [c], Kun Zhang [c], Zhangjian Zhou [a,*]

[a] School of Materials Science and Engineering, University of Science and Technology Beijing, Beijing 100083, China
[b] National Engineering Laboratory for Hydrometallurgical Cleaner Production Technology, CAS Key Laboratory of Green Process and Engineering, Institute of Process Engineering, Chinese Academy of Sciences, Beijing 100190, China
[c] Institute of Mechanics, Chinese Academy of Sciences, Beijing 100190, China

ARTICLE INFO

Keywords:
W based heavy alloys
Gradient structure
Electrodeposition
Core–shell composite powder
W–W contiguity
Particle coalescence
Solution–reprecipitation

ABSTRACT

W–Ni–Fe heavy alloys were obtained by liquid–phase sintering of W@NiFe composite powders. The face–centered cubic NiFe alloys were deposited as a shell on the core of tungsten particle to form W@NiFe composite powders by intermittently electrodeposition. After liquid–phase sintering, W–Ni–Fe heavy alloys had more gradient morphology and shape distortion as the holding time increased. The bending strength and hardness distributed graded at 1470 °C holding for 0.5 h. Top layer of gradient W–Ni–Fe heavy alloys at 1470 °C holding for 0.5 h showed low W—W contiguity, no normal growth of W particle size and high sintered density, which led to excellent bending strength (1245 MPa) and hardness (340 $HV_{0.2}$). The structure and composition of W@NiFe composite powders and the optimization of sintering process parameters were analyzed and discussed. The sintering behavior of W@NiFe composite powders were also investigated in details.

1. Introduction

W–Ni–Fe heavy alloy is a kind of composite material, in which hard body–centered cubic (bcc) W particles were embedded in ductile face–centered cubic (fcc) Ni–Fe–W solid solution alloys. It is widely used as kinetic energy penetrators, radiation shields, counter weights due to their high density, high strength, and easy machinability. The comprehensive mechanical properties of W–Ni–Fe heavy alloys also need to be considered. It is related to the size of original W particles, porosity, W—W contiguity and many other factors [1,2]. The high degree of contiguity of tungsten is easy to be inherited from the powder mixing step, which results in the embrittlement of W–Ni–Fe heavy alloys [3]. Therefore, powder mixing has been a crucial technique in obtaining W–Ni–Fe heavy alloys with low W—W contiguity which includes ball milling [4], spray drying [5], soft chemical method [6], electrodeposition [7,8] and so on, to fabricate composite powders. Among these, high–energy ball milling can obtain fine–grained W–Ni–Fe composite powders [4,9]. But this method is easy to introduce impurities. Fine W–Ni–Fe composite powders without impurities can be obtained by spray–drying and hydrogen reduction [5]. However, the complexity of this method restricts mass production. Recently, we have proposed an electrodeposition process, called intermittently electrodeposition to realize powder plating [10,11]. It is considered as a promising method to produce core–shell composite powders with high purity and unique structure [11,24], and can be mass produced. In our previous work, W—Cu core–shell composite powders were effective to fabricate W—Cu composites with homogeneous phase distribution and low W—W contiguity [24].

W–Ni–Fe heavy alloys with gradient structure are considered as desired materials to improve penetration performance in penetrator core materials [12]. In this way, the penetrator could obtain high enough hardness on the surface and appropriate toughness inside [13]. Usually, additional post–treatments, such as carburizing [13] or diffusing of Mo [14] on the surface of W–Ni–Fe alloys are employed to obtain gradient structure with high hardness on the surface of W–Ni–Fe alloys. However, very few reports were focused on the preparation of gradient structure directly for heavy alloys using W–Ni–Fe composite powder. In this work, W@NiFe composite powders (W@NiFe is equal to W coated with NiFe alloys) have been used to fabricate gradient W–Ni–Fe heavy alloys by liquid–phase sintering. The intermittently electrodeposition method deposited a NiFe–shell covering micron W particle which differed from the traditional powders reported in [7,8,15,16]. The microstructure and phase structure of W@NiFe composite powder were analyzed. The microstructure and mechanical

* Corresponding author.
E-mail address: zhouzhj@mater.ustb.edu.cn (Z. Zhou).

https://doi.org/10.1016/j.ijrmhm.2020.105447
Received 2 October 2020; Received in revised form 19 November 2020; Accepted 19 November 2020
Available online 21 November 2020

properties of sintered composite as well as sintering behaviors of W@NiFe composite powder were discussed in details.

2. Experiment procedure

2.1. Fabrication of W@NiFe composite powders and gradient W–Ni–Fe heavy alloys

A pure copper plate (purity of 99.99%) with external diameter of 180 mm was used as a cathode plate. Iron plate (purity of 99.9%) with 120 × 10 × 2 mm^3 and nickel plate (purity of 99.9%) with 120 × 80 × 2 mm^3 were used as anode plates. W powders with average particle size of ~6 μm and purity of 99.9% were used as the starting materials. The cathode plate covered with W particles was attached to the bottom of a homemade cylindrical electroplating tank which was full of electroplating baths. The anode plate and cathode plate were placed in parallel with distance of 100 mm. Firstly, stir the W powders using a stirring device. After finishing stirring, turn off it. Then secondly, turn on one other device energized for electrodeposition. When electrodeposition was completed, turned off the power and restarted to stir, thus the whole W powders, not only powders floated on the surface of electroplating baths, could be deposited. This is one cycle for intermittently electrodeposition. And the W@NiFe composite powders could be obtained after several cycles. Finally, wash the W@NiFe composite powders with deionized water and absolute ethanol, and vacuum–dry at 60 °C for 30 min. Details of the process also can be found in our previous works [14,27]. Compositions of plating bath solution are shown in Table 1. Electrodeposition parameters are shown in Table 2. The duty cycle and average current density (I_{avg}) were calculated by Eqs. (1) and (2).

$$\text{Duty cycle} = \frac{t_{on}}{t_{on} + t_{off}} \tag{1}$$

Where t_{on} is deposition time, t_{off} is agitating time.

$$I_{avg} = \frac{t_{on}}{t_{on} + t_{off}} \times I \tag{2}$$

Where I is current density at deposition time.

The W@NiFe composite powders were uniaxially compacted under 300 MPa, then sintered in a tube furnace under different sintering conditions, including 1300 °C for 1.5 h, 1400 °C for 1.5 h and 3 h, and 1470 °C for 0.5 h, 1 h, 2 h in an Argon atmosphere. After sintering, the samples were cooled at a rate of 15 °C/min to 800 °C and then furnace cooled in Argon.

2.2. Characterizations

The morphologies of W@NiFe composite powders and sintered composites were observed by field–emission scanning electron microscope (JSM–7001F). The phase structures were analyzed by X–ray diffraction (Smart Lab (9 KW)) with Cu Kα radiation (λ = 1.5418 Å) and operated at 45 kV and 200 mA. Chemical compositions of W@NiFe composite powders were identified by X–ray Fluorescence Spectrometer (XRF). The density of sintered composites was determined by Archimedes' method. The theoretical density of the W@NiFe composite powders was used as the theoretical density of bulk composites. The particle size distribution of W@NiFe composite powders and original W particles was detected by Dynamic image analysis (Camsizer X2). The particle size of W in sintered composites was detected by Nano Measurer 1.2 software. The hardness was measured using a Vickers hardness tester at 200 g load holding for 15 s. The bending strength was measured by using three–point bending test samples of which size was 12.0 mm × 2 mm × 1 mm. The bending strength σ (MPa) was calculated by Eq. (2.3-1):

$$\sigma = \frac{3FL}{2bh^2} \tag{2.3-1}$$

Where F is the maximal bending force (N), L is the length of sample (mm), b is the width of sample (mm) and h is the thickness of sample (mm).

The W—W contiguity C_{WW} was estimated by Eq. (2.3-2) [17]:

$$C_{WW} = \frac{2N_{WW}}{N_{WM} + 2N_{WW}} \tag{2.3-2}$$

Where N_{WW} is the number of W—W interfaces and N_{WM} is the number of W–Ni/Fe.

We observed microstructure and measured bending strength of the gradient sintered specimens along the direction of gravity that was from top, middle to bottom. The bottom of sample was broken after holding for 2 h.

Table 1
Composition of the plating bath solution.

Agent	Formula	Role in bath solution	Concentration (g/L)
Nickel sulfate	$NiSO_4{\cdot}6H_2O$	Nickel ions	60
Ferrous sulfate	$FeSO_4{\cdot}7H_2O$	Ferrous ions	20
Boric acid	H_3BO_3	Buffering solution	40
Sodium chloride	NaCl	Chloride	10
Dodecyl sodium sulfate	$NaC_{12}H_2S_5O_4$	Stabilizing agent	0.1
Ascorbic acid	$C_6H_8O_6$	Stabilizing agent	1
Trisodium citrate dihydrate	$C_6H_5Na_3O_7{\cdot}2H_2O$	Stabilizing agent	20
D–Glucose	$C_6H_{12}O_6{\cdot}H_2O$	Stabilizing agent	3

Table 2
Electrodepostion parameters in this study.

Temperature/K	PH	I_{avg}/A/dm^2	T_{on}/s	T_{off}/s	Duty cycle	Cycle
328	3.5	0.71, 1.42, 2.13, 3.55	240	100	0.71	10

3. Result and discussion

3.1. Microstructure of W@NiFe composite powders

The surface morphology and cross section morphology of the fabricated core–shell powders can be seen in Fig. 1 (a) and (c) respectively. Ni and Fe shell layer distributed in the core of W particles evenly. No distinct pores or cracks could be observed along the interface between W core and NiFe shell. The particle size distribution of W@NiFe composite powders at different current density is shown in Fig. 1(b). The particle size of W@NiFe composite powders increased with current density under the same electrodeposition condition. These unsmooth curves show the aggregation in composite powders, especially in original W particles. Only one strong peak presents at the average current density lower than 2.13 A/dm^2. However, more than two peaks appear at 3.55 A/dm^2 indicating extremely non–homogeneous particle distribution at high current density.

3.2. Phase structure

Fig. 2 shows X–ray diffraction (XRD) patterns of W powders and W@NiFe composite powders obtained at different average current density. The strong W peaks appeared in all samples with corresponding 2 θ at 40.264° (110), 58.274° (200), 73.195° (211) and 87.021° (220). W@NiFe composite powders have major NiFe solid solution peaks at 2θ which is equal to about 43.494° (111) and 50.673° (200), as seen in the inserted picture of Fig. 2. The intensity of NiFe solid solution peaks

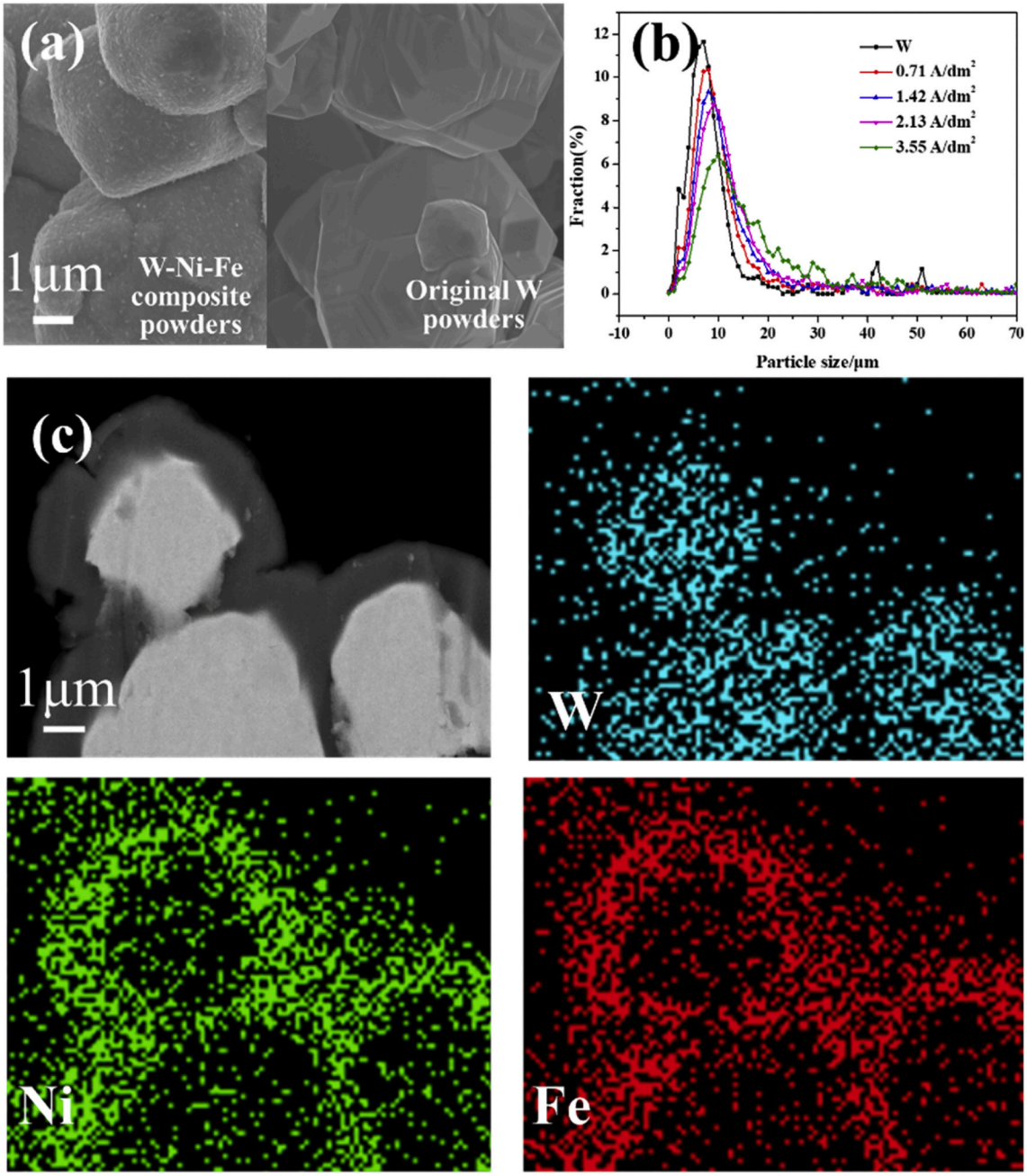

Fig. 1. (a) SEM images of W@NiFe composite powders, (b) particle size distribution of W@NiFe composite powders obtained at average current density of 0.71, 1.42, 2.13 and 3.55 A/dm^2, (c) Cross–section of W@NiFe composite powder at average current density of 0.71 A/dm^2 with map scanning.

increased with iron concentration. NiFe alloys had face–centered cubic structure (fcc) at low iron content (less than 35 at. %) based on Fe—Ni phase diagram [19]. This result agreed well with the reported work in [18,19]. Research showed that W–Ni–Fe heavy alloys with 90–93 wt%W and Ni to Fe of 7:3 benefit mechanical properties at the high strain rate [20]. Therefore, W@NiFe composite powders at average current density of 2.13 A/dm^2 were used as raw material to fabricate bulk composites under various sintering conditions. The compositions of W@NiFe composite powders at average current density of 2.13 A/dm^2 were 89.071 wt % W, 7.706 wt% Ni and 3.223 wt% Fe.

3.3. Sintering behavior under different sintering conditions

Fig. 3 shows relative density and mean W particle size of W–Ni–Fe heavy alloys that were consolidated under different sintering conditions. The relative density of sintered composites increases from 1300 °C to 1400 °C, and reaches a maximal value of 99.5% at 1470 °C, as seen in Fig. 3(a). W–Ni–Fe heavy alloys changed from solid–state to liquid–state when sintering temperature was higher than 1400 °C [22]. Insufficient sintering kinetic energy resulted in high porosity when sintered at 1400 °C, especially at 1300 °C. Fig. 3(b) depicts W particle size of sintered W–Ni–Fe heavy alloys under different sintering conditions. The W particle size of sintered W–Ni–Fe heavy alloys presented self–similarity when sintering temperature was lower than 1470 °C. It was interesting to find that the W particle size showed graded distribution in the sample sintered at 1470 °C for 0.5 h. If prolonged sintering time to 1 h, the graded distribution will be more obvious. W particle size decreased in the top and middle layer, increased in the bottom layer. If extended holding time to 2 h, the graded distribution disappeared and the W particle size became about five times bigger than the original particle

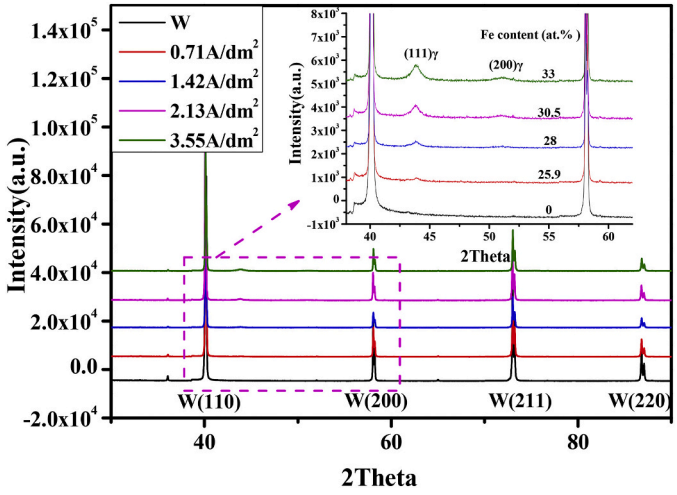

Fig. 2. XRD patterns of the W particles and W@NiFe composite powders obtained at average current density of 0.71, 1.42, 2.13, 3.55 A/dm^2. Nomenclature: γ– face–centered cubic.

size.

Figs. 4 and 5 show morphologies of cross section and fracture surface of sintered W–Ni–Fe heavy alloys under different sintering conditions. Cross–section images are electron back–scattering micrographs. The bright areas are W–rich phases while the gray areas are NiFe–rich phases. Obvious growth of W particle, together with shape rounding and disappearance of distinct pores, can be found while changing from solid–state sintering to liquid–state sintering. The microstructure of sintered W–Ni–Fe heavy alloys show the gradient structure along gravity after sintering at 1470 °C for 0.5 h and 1 h, as seen in Fig. 4(e) and (f). The W particle size, W—W contiguity and volume fraction of solid increased along the direction of gravity. This phenomenon was also observed in previous studies [21]. The increase in W particle size and W—W contiguity resulted in a more uneven distribution of liquid phase in gradient sample by extending holding time to 1 h. The microstructure of sample with larger W particle became homogeneous after sintering for 2 h.

3.4. Mechanical property of sintered W–Ni–Fe heavy alloys

The bending strength and W—W contiguity of sintered W–Ni–Fe heavy alloys are shown in Fig. 6. The bending strength increased with sintering temperature following the rise of sintered density. Samples which were sintered at 1300 °C and 1400 °C showed rather uniform bending strength at a lower value. For samples sintered at 1470 °C for 0.5 h and 1 h, the bending strength decreased from top layer to bottom layer, which was due to the formation of gradient microstructure along the direction of gravity during liquid–phase sintering (Fig. 4(e) and (f)). The growth of W particle size aggravated the connection between W particles (Fig. 6(b)) in sintered W–Ni–Fe heavy alloys, which showed more *W*/W interfacial debonding in fracture morphologies (Fig. 5(e) and (f)). In other words, the main fracture mode transferred from W cleavage and matrix rupture to W/W interfacial debonding along the direction of gravity. The top layer of the W–Ni–Fe heavy alloys sintered at 1470 °C for 0.5 h showed excellent bending strength, about 1245 MPa, which was due to low W—W contiguity, no abnormal growth of W particle size and high sintered density. The hardness of that sample showed a gradient along the direction of gravity, and the hardness value ranged from 340 $HV_{0.2}$ to 316 $HV_{0.2}$.

Interestingly, although W particle size in the top layer of sample sintered at 1470 °C for 1 h was smaller accordingly (Fig. 3(b)), the bending strength was lower than the sample sintered at 1470 °C for 0.5 h (Fig. 6). The previous work showed that the mechanical properties of W based heavy alloys were related to not only W particle size and W—W contiguity, but also matrix volume fraction [7]. From Fig. 4(e) and (f), the top layer of sample sintered at 1470 °C for 1 h has a larger matrix volume fraction resulting in lower bending strength. After being sintered at 1470 °C for 2 h, the bending strength became even and higher than the sample sintered at 1300 °C and 1400 °C respectively. Anyway, it was lower than the maximal value of gradient sample because of the growth of W particle size.

3.5. Densification mechanism W@NiFe composite powders

Schemes of densification process of W@NiFe composite powder are shown in Fig. 7. At solid–state sintering stage, diffusion controlled the neck growth. After NiFe alloys were coated on the surface of W particles, the shell of NiFe alloys was easy to diffuse and formed sintering necks (Fig. 7(a) and (b)). Whereas W particles maintained initial size when the temperature was below 1400 °C (Fig. 3 and Fig. 4(a) and (b)). The sintered W–Ni–Fe heavy alloys showed very low W—W contiguity but high porosity at low sintering temperature in case that the sintering time was short. As seen in Fig. 4(b) and (c), prolonging holding time can promote the growth of sintering necks resulting in the rise of W—W contiguity (Fig. 7(c)). At liquid–phase sintering stage, about 22 wt% [22] of W could solute in NiFe phase theoretically and spheroidization appeared. Besides that, the dissolution of W could promote densification further and maintain low W—W contiguity in final sintered composites [23]. After long holding time, the formation of closed pore reduced relative density. These closed pores in final sample were due to the coalescence of W particle that limits particle rearrangement.

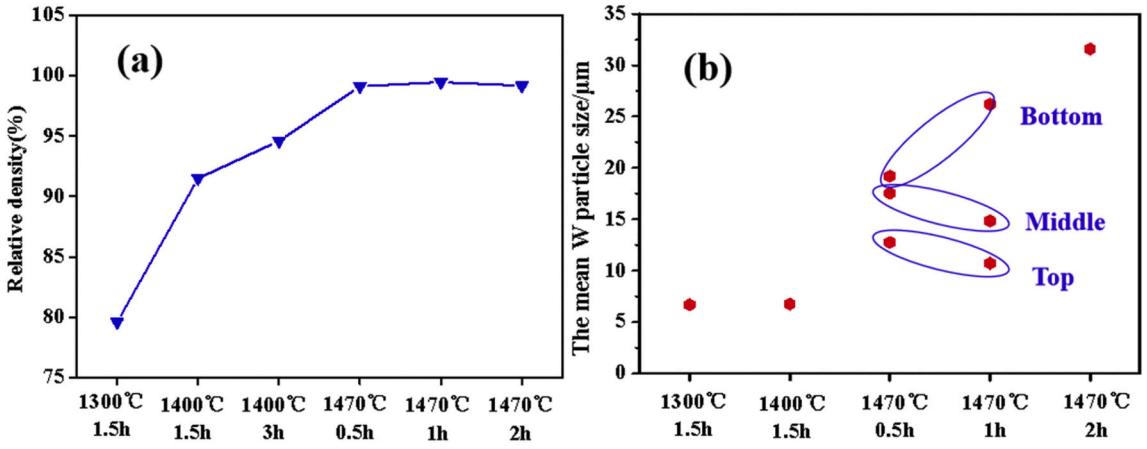

Fig. 3. The relative density and the mean W particle size of W–Ni–Fe heavy alloys prepared with various sintering parameters.

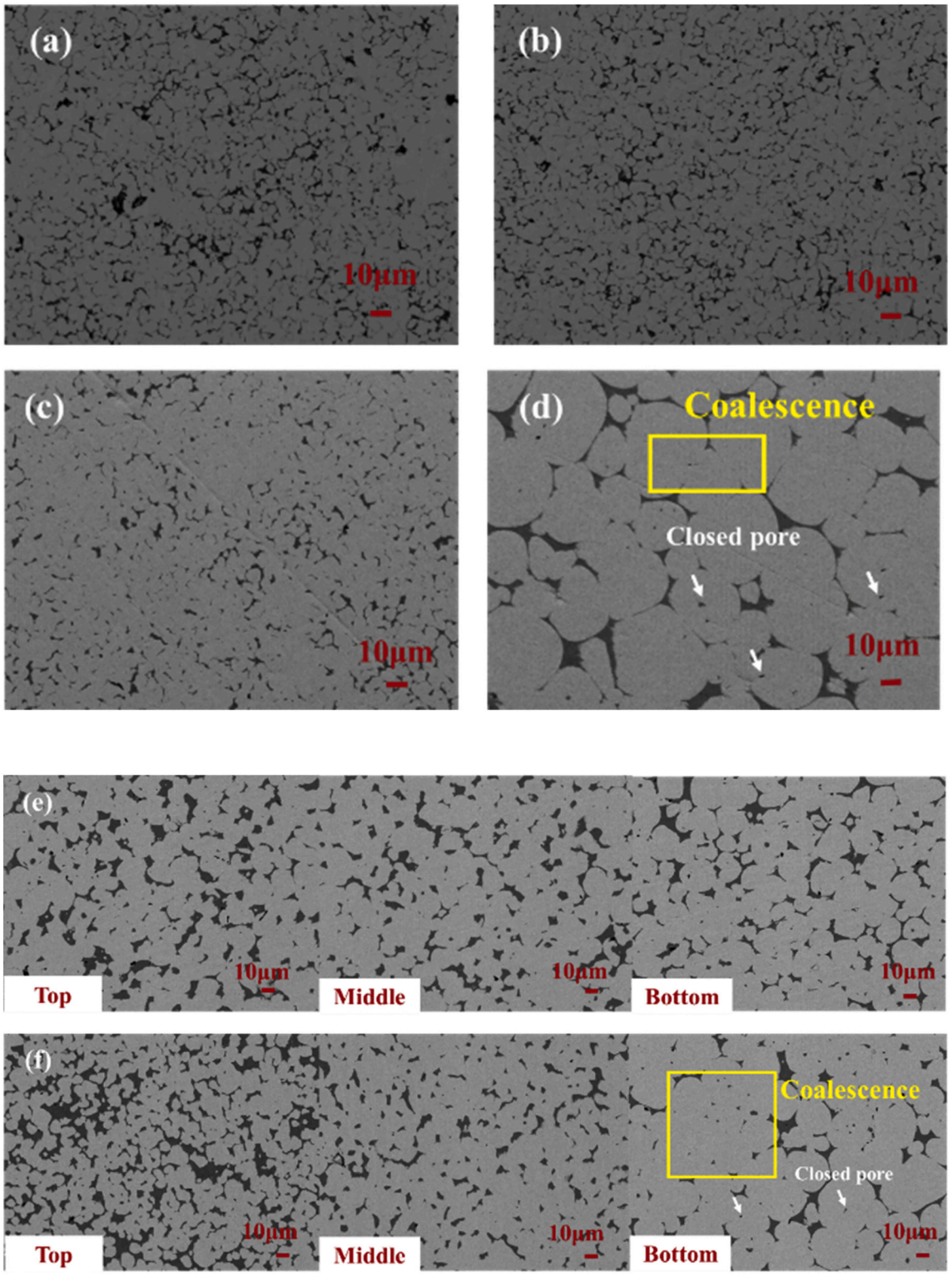

Fig. 4. The SEM images of W–Ni–Fe heavy alloys prepared with various sintering parameters (a) 1300 °C–1.5 h, (b) 1400 °C–1.5 h, (c) 1400 °C–3 h, (d) 1470 °C–2 h, (e) 1470 °C–0.5 h from left to right: gradient along the direction of gravity and (f) 1470 °C–1 h from left to right: gradient along the direction of gravity.

At liquid–phase sintering stage, the LSW (Lifshitz and Slyozov and Wagne) theory shows that the W particle size (G) increase with sintering time (t).

$$G^n = G_0{}^n + kt \tag{3.4-1}$$

Where G_0 is initial W particle size, k is growth rate constant, n is grain growth exponent, Exponents with generally a value near 3 are most common, especially for tungsten–heavy alloy [24]. In this work, G_0 was neglected because W particle size in sintered composite (at 1470 °C holding for 2 h) got five times than original particles. Taking the ln of both side of Eq. (3.4-1):

$$lnG = lnk/n + lnt/n \tag{3.4-2}$$

The relationship between lnG and lnt at 1470 °C holding for 30 min,

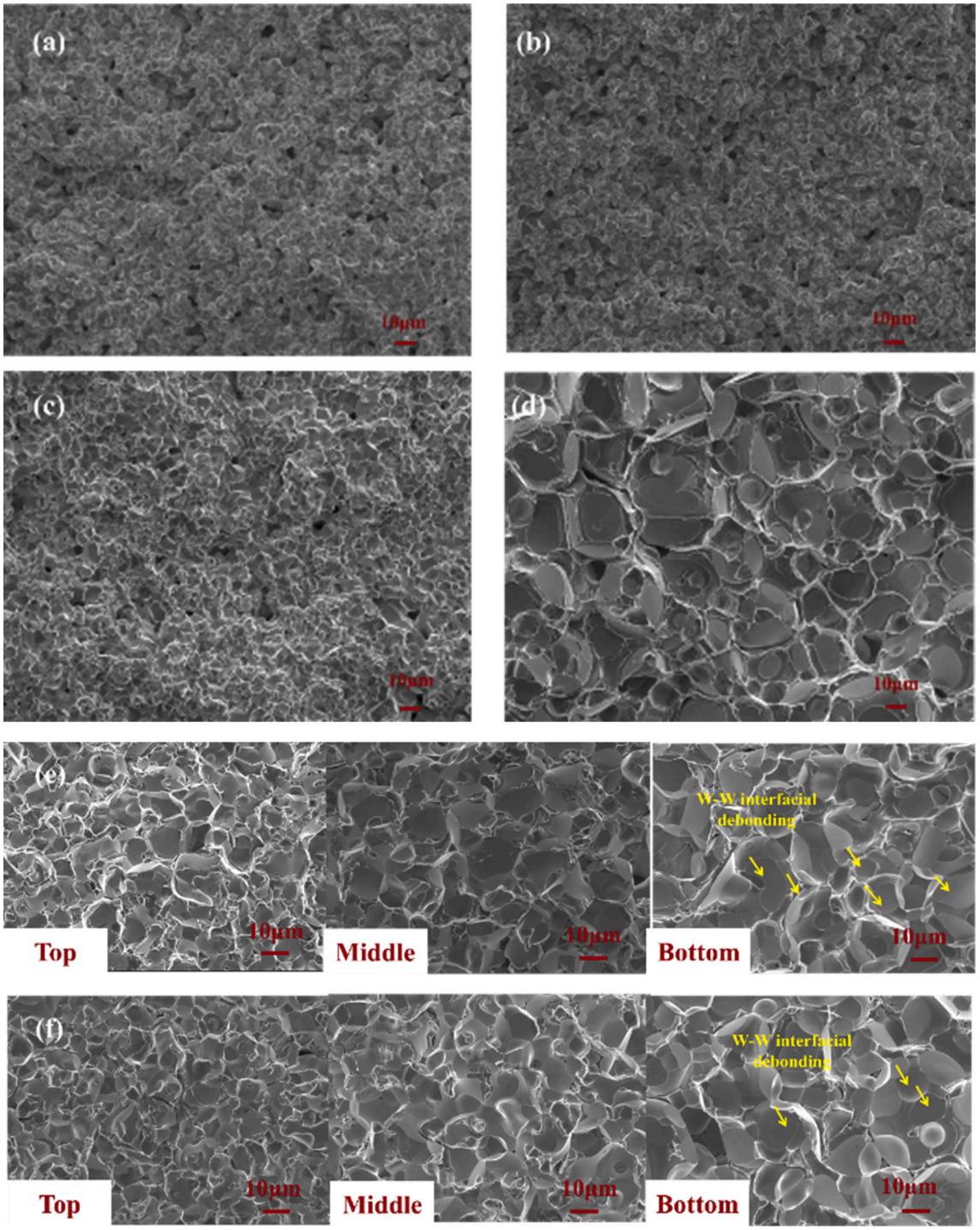

Fig. 5. Fracture morphologies of W–Ni–Fe heavy alloys prepared with various sintering parameters (a) 1300 °C–1.5 h, (b) 1400 °C–1.5 h, (c) 1400 °C–3 h, (d) 1470 °C–2 h, (e) 1470 °C–0.5 h from left to right: gradient along the direction of gravity and (f) 1470 °C–1 h from left to right: gradient along the direction of gravity.

60 min and 120 min are showed in Fig. 8. $n = 2.86$ can be calculated by fitting line. n ≈ 3 was considered as solution–reprecipitation controlled grain growth [24,25]. In such cases the growth rate constant is given by [26].

$$k = \frac{8\chi_0 \sigma V_m^2 D}{9RT} f(V_s) \tag{3.4-3}$$

Where χ_0 is equilibrium solubility, σ is the interfacial energy between particle and matrix, V_m is the molar volume fraction of particle, $f(V_s)$ is the volume fraction modification parameter, D is diffusivity of the solute (tungsten) in the liquid, R is gas constant and T is temperature. The growth rate increases with volume of particle. Stratification occurs because of gravity during liquid phase sintering resulting in higher solid volume fraction at bottom of sample. Coalescence would be a significant coarsening mechanism when solid fraction is high [26]. As seen in Fig. 5 (e) and (f), more W—W interfacial debonding appear at bottom of samples. At initial liquid phase sintering, core–shell powder was benefit for homogeneity of phase distribution which had been already confirmed in our previous work [27]. The difference of microstructure at top and bottom was not obvious at holding time of 0.5 h. However, the

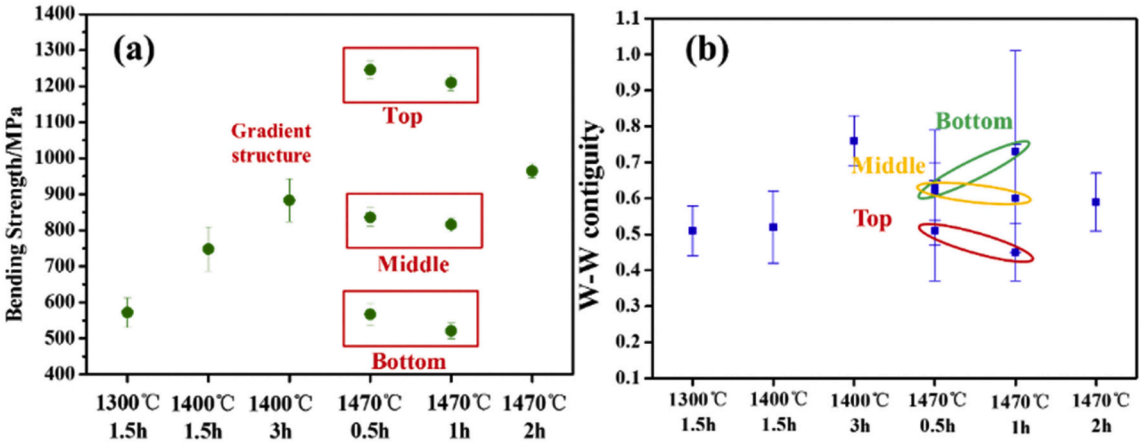

Fig. 6. (a) The bending strength and (b) W—W contiguity of sintered W–Ni–Fe heavy alloys prepared under various sintering conditions.

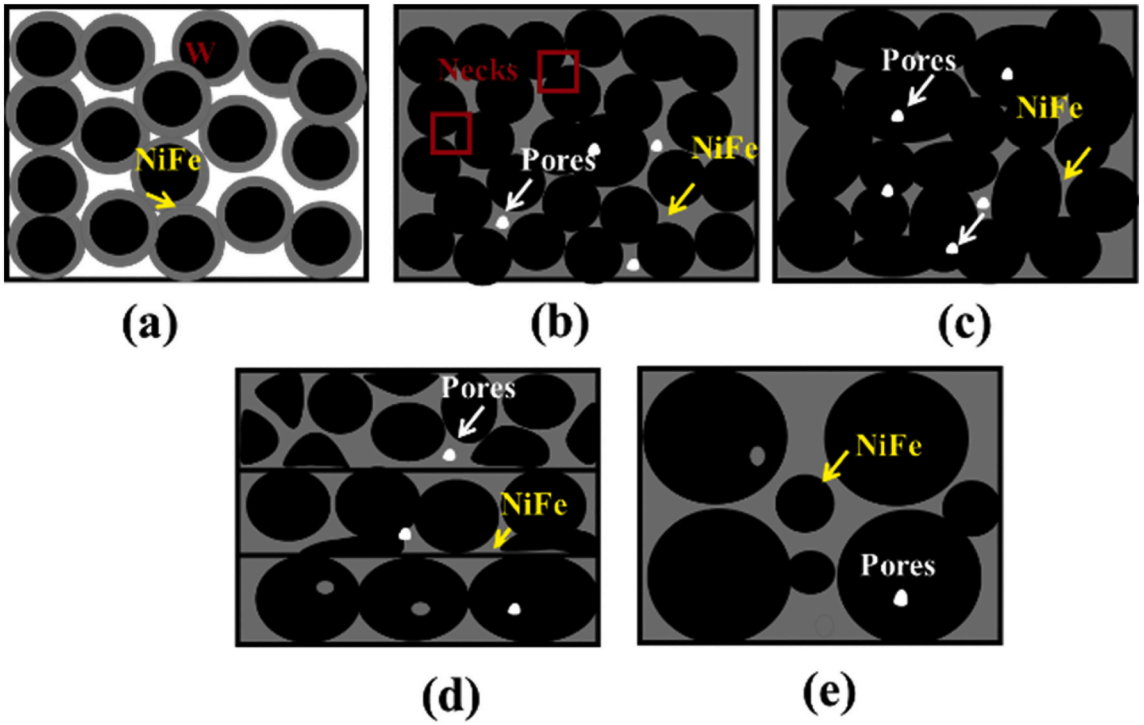

Fig. 7. The schematic densification process: (a) green compact with high porosity; (b) sintering necks formation at initial solid–phase sintering stage: W@NiFe composite powders connected with each other, low W—W contiguity and high porosity; (c) the sintering neck grew and W—W contiguity increased at elevated sintering time during solid–phase sintering process; (d) gravity led to stratification effects; (e)The W—W contiguity decreased and W particle size increased in final sintered sample at long sintering time. Particle coalescence and solution–reprecipitation process worked together to get microstructure homogeneity and densification. (For interpretation of the references to colour in this figure legend, the reader is referred to the web version of this article.)

difference of W particle size and W—W contiguity effected significantly bending strength and hardness. The main particle growth mechanism of each layer was particle rearrangement and solution–reprecipitation due to sufficient liquid content in short–term liquid phase sintering. Increasing the sintering time to 1 h, the main particle growth mechanism was solution–reprecipitation and coalescence at top and bottom of sample respectively. This is due to gravity that causes the liquid content of the top layer to be higher than that of the bottom layer. Consequently, the microstructure at top and bottom of sample showed a significant difference (Fig. 7(d)). After sintering for 2 h, a more homogeneous microstructure formed with bigger W particle size and a few closed pores due to the cooperation of coalescence and solution–reprecipitation (Fig. 7(e)).

Dimensional control is one of the prime concerns in consolidating composite by liquid phase sintering. The shape distortion in W–Ni–Fe heavy alloys liquid phase sintered at 1470 °C for 0.5 h and 1 h is given in Fig. 9. A typical elephant–foot profile is more distinct after holding for 1 h. Reports [21] showed that higher solid content provides a connected solid skeletal network leading to structural rigidity of the compact. It can be concluded that it will obtain a sintered composite with higher structural rigidity by using core–shell powder with incomplete covering. In this way, it can ensure the uniform distribution of different phases and formation solid skeletal network at the same time. At present, W–Ni–Fe alloys with gradient hardness and bending strength can be obtained by direct liquid–phase sintering using W@NiFe core–shell powder when the temperature is 1470 °C holding for 0.5 h. This gradient material is

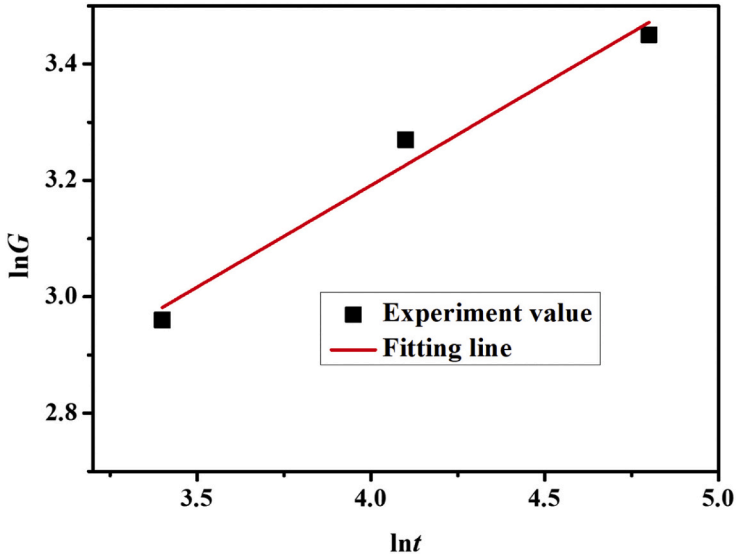

Fig. 8. Relationship between ln$G$ and ln$t$ at 1470 °C holding for 30 min, 60 min and 120 min.

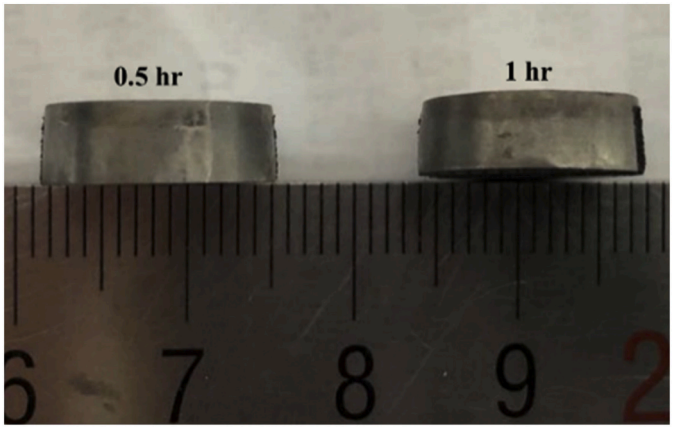

Fig. 9. Shape distortion in W–Ni–Fe heavy alloys after liquid phase sintered at 1470 °C for 0.5 h and 1 h.

expected to improve the penetration performance in penetrator core materials. In next study, we will discuss the influence of powder cladding rate on shape distortion. Meanwhile, we will measure multiple data points for a deeper studying of sintering kinetic and make the exponents with greater confidence [28].

4. Conclusions

W–Ni–Fe heavy alloys were fabricated by liquid–phase sintering of W@NiFe composite powders. The conclusions are presented below:

(1) W@NiFe composite powders were prepared by intermittently electrodeposition. The face–centered cubic NiFe alloys were deposited on the core of W particles. No pores or cracks were observed at the W–NiFe interface.
(2) The sintered W–Ni–Fe heavy alloys showed a distinct gradient structure after liquid–phase sintering at 1470 °C with holding time of 1 h. The microstructure will be homogeneous if prolonging the sintering to 2 h. The sintering mechanism involved solution–reprecipitation process and particle coalescence, worked in different layers of the gradient sample.
(3) The bending strength and hardness of W–Ni–Fe heavy alloys sintered at 1470 °C with holding time of 0.5 h showed graded distribution due to the differences in W particle size and W—W contiguity after liquid–phase sintering. The value of bending strength and hardness at the top layer of gradient W–Ni–Fe heavy alloys reached 1245 MPa and 340 $HV_{0.2}$ because of no abnormal growth of W particle size, low W—W contiguity and high sintered density.

Declaration of Competing Interest

The authors declare no competing financial interest.

Acknowledgments

This work was financially supported by National Key Research and Development Program of China (No. 2017YFC0703205) and National Natural Science Foundation of China (No. 51501179 and No. 11802309).

References

[1] A. Muthuchamy, D.V. Yadav, D.K. Agrawal, et al., Structure–property correlations of W–Ni–Fe–Mo heavy alloys consolidated using spark plasma sintering, Mater. Res. Express 6 (2018) 1–5.
[2] U.R. Kiran, A. Pancha, M. Sankaranarayana, GVSN Rao, T K Nandy, effect of alloying addition and microstructural parameters on mechanical properties of 93% tungsten heavy alloys, Mater. Sci. Eng. A 640 (2015) 82–90.
[3] S. Eroglu, T. Baykara, Effects of powder mixing technique and tungsten powder size on the properties of tungsten heavy alloys, J. Mater. Process. Technol. 103 (2000) 288–292.
[4] Ho J. Ryu, Soon H. Hong, Woon H. Baek, Microstructure and mechanical properties of mechanically alloyed and solid–state sintered tungsten heavy alloys, Mater. Sci. Eng. A 291 (2000) 91–96.
[5] J.L. Fan, X. Gong, B.Y. Huang, M. Song, T. Liu, J.M. Tian, Densification behavior of nanocrystalline W–Ni–Fe composite powders prepared by sol–spray drying and hydrogen reduction process, J. Alloys Compd. 489 (2010) 188–194.
[6] Y. Liu, J.G. Cheng, Y.M. Fan, L. Wan, W.C. Chen, J.F. Li, Preparation of W–Ni–Fe heavy alloys by soft chemical method, Mater. Res. Innov. 19 (2015) S5–689-S5-693.
[7] M. Spasojević, L. Ribić-Zelenović, A. Maričić, P. Spasojević, Structure and magnetic properties of electrodeposited Ni87.3Fe11.3W1.4 alloy, Powder Technol. 254 (2014) 439–447.
[8] L. Ribić-Zelenović, N. Ćirović, M. Spasojević, N. Mitrović, A. Maričić, V. Pavlović, Microstructural properties of electrochemically prepared NiFe–W powders, Mater. Chem. Phys. 135 (2012) 212–219.
[9] D.P. Xiang, L. Ding, Y.Y. Li, G.B. Chen, Y.W. Zhao, Preparation of fine–grained tungsten heavy alloys by spark plasma sintered W–7Ni–3Fe composite powders with different ball milling time, J. Alloys Compd. 562 (2013) 19–24.
[10] Z.J. Zhou, P. Wu, J.Q. Li, B.J. Liu, Chinese Patent, CN104999077B, 2015 (in Chinese).

[11] J.Q. Li, N. Deng, P. Wu, Z.J. Zhou, Elaborating the Cu–network structured of the W–Cu composites by sintering intermittently electroplated core–shell powders, J. Alloys Compd. 770 (2019) 405–410.
[12] J. Zhu, S. Cao, H. Liu, Fabrication of W–Ni–Fe alloys with gradient structures, Int. J. Refract. Met. Hard Mater. 36 (2013) 72–75.
[13] J. Sug-Woo, K. Dong-Kuk, L. Sunghak, N. Joon-woong, K. Suk-Joong, Effect of surface carburization on dynamic deformation and fracture of tungsten heavy alloy, Metal. Mater. Trans. A 30 (1999) 2027–2035.
[14] Y. Jin, S.H. Cao, J. Zhu, H.Y. Liu, B.H. Chen, H. Xu, Gradient structure induced by molybdenum in 90W–Ni–Fe heavy alloy, Int. J. Refract. Met. Hard Mater. 43 (2014) 141–146.
[15] F.J. He, J. Yang, T.X. Lei, C.Y. Gu, Structure and properties of electrodeposited Fe–Ni–W alloys with different levels of tungsten content: a comparative study, Appl. Surf. Sci. 253 (2007) 7591–7598.
[16] M. Donten, H. Cesiulis, Z. Stojek, Electrodeposition and properties of NiW, FeW and FeNiW amorphous alloys: a comparative study, Electrochim. Acta 45 (2000) 3389–3396.
[17] X.Q. Li, K. Hu, S.G. Qu, L. Li, C. Yang, 93W–5.6Ni–1.4Fe heavy alloys with enhanced performance prepared by cyclic spark plasma sintering, Mater. Sci. Eng. A 599 (2014) 233–241.
[18] C.W. Su, E.L. Wang, Y.B. Zhang, F.J. He, $Ni_{1-x}Fe_x$ ($0.1 < x < 0.75$) alloy foils prepared from a fluorborate bath using electrochemical deposition, J. Alloys Compd. 474 (2009) 190–194.
[19] T.R. Lee, L.W. Chang, C.H. Chen, Effect of electrolyte temperature on composition and phase structure of nanocrystalline Fe–Ni alloys prepared by direct current electrodeposition, Surf. Coat. Technol. 207 (2012) 523–528.
[20] K. Hu, X.Q. Li, X. Ai, X.G. Qu, Y.Y. Li, Fabrication, characterization, and mechanical properties of 93W–4.9Ni–2.1Fe/95W–2.8Ni–1.2Fe–$1Al_2O_3$ heavy alloy composites, Mater. Sci. Eng. A 636 (2015) 452–458.
[21] R. Bollina, R.M. German, Heating rate effects on microstructural properties of liquid phase sintered tungsten heavy alloys, Int. J. Refract. Met. Hard Mater. 22 (2004) 117–127.
[22] Y.B. Zhu, Y. Wang, X.Y. Zhang, G.W. Qin, W/NiFe phase interfacial characteristics of liquid–phase sintered W–Ni–Fe alloy, Int. J. Refrac. Metals Hard Mater. 25 (2007) 275–279.
[23] S.J. Park, J.F. Guo, J.L. Johnson, R.M. German, Densification behavior of tungsten heavy alloy based on master sintering curve concept, Metal. Mater. Trans. A 37 (2006) 2837–2848.
[24] R.M. German, A. Griffo, Y. Liu, Gravitational effects on grain coarsening during liquid–phase sintering, Metal. Mater. Trans. A 28 (1997) 215–221.
[25] A. Bose, R.M. German, Microstructural refinement of W–Ni–Fe heavy alloys by alloying additions, Metall. Trans. A. 19 (1988) 3100–3103.
[26] Sung Chul Yang, S.S. Mani, R.M. German, The effect of contiguity on growth kinetics in liquid–phase sintering, JOM 42 (1990) 16–19.
[27] N. Deng, Z. Zhou, J. Li, Y. Wu, W–cu composites with homogeneous cu–network structure prepared by spark plasma sintering using core–shell powders, Int. J. Refract. Met. Hard Mater. 82 (2019) 310–316.
[28] J.D. Bolton, A.J. Gant, Microstructural development and sintering kinetics in ceramic reinforced high speed steel metal matrix composites, Powder Metall. 40 (1997) 143–151.